CHEMISTRY OF MATERIALS

pubs.acs.org/cm

Article

Epitaxial Growth of Atomic-Layer Cu on Pd Nanocatalysts for Electrochemical CO_2 Reduction

Published as part of Chemistry of Materials special issue "In Memory of Prof. Francis DiSalvo".

Shikai Liu,[#] Chuqiao Shi,[#] Chaokai Xu, Haichuan Zhang, Wenqi Li, Valentín Briega-Martos, Qian He, Yimo Han,* and Yao Yang*

Cite This: *Chem. Mater.* 2025, 37, 290−296

Read Online

ACCESS | Metrics & More | Article Recommendations | Supporting Information

ABSTRACT: CO_2 reduction reaction (CO_2RR) facilitates the sustainable synthesis of fuels and chemicals. Although copper (Cu) enables CO_2-to-multicarbon product (C_{2+}) conversion, Cu-based electrocatalysts, particularly nanocatalysts, face challenges in poor selectivity and stability owing to the highly dynamic nature of Cu atoms under reaction conditions. Core−shell structures present a promising approach to address these issues by modulating the Cu overlayer−substrate interactions with atomic-level precision. Here, we report on Pd@Cu core−shell structures with atomically thin and nanometer-thick Cu overlayers on single-crystal Pd nanocubes with {100} facets promoting the CO_2-to-C_{2+} conversion. The microstructures and surface compositions at the atomically sharp Pd/Cu interface were investigated by atomic-scale scanning transmission electron microscopy (STEM) imaging and electron energy-loss spectroscopy (EELS). Our results reveal that atomic-layer Cu epitaxially grows on Pd and adapts to the lattice of the Pd substrate. The reaction-driven migration of atomic-layer Cu is effectively suppressed on Pd due to the strong Cu−Pd interaction. While Pd only reduces CO_2 to C_1 products, atomic-layer Cu on Pd can initiate the C_{2+} production during the CO_2RR. Thick Cu overlayers (∼15 nm) on Pd further enhance the C_{2+} faradaic efficiency while undergoing significant structural reconstruction, with only the 2−3 nm Cu layers near the Pd surface remaining stable and resistant to Cu migration after the CO_2RR. We anticipate that Pd@Cu core−shell structures with intermediate Cu shell thickness hold significant potential for enhancing C_{2+} selectivity while maintaining high stability of nanocatalysts for CO_2 reduction to liquid fuels.

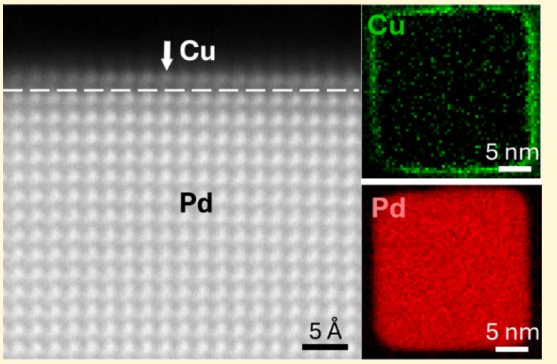

INTRODUCTION

The electroreduction of CO_2 to higher-value chemicals offers significant potential for mitigating climate change and advancing the chemical industry toward carbon neutralization.[1] Among various heterogeneous electrocatalysts, copper (Cu) stands out for its unique ability to convert CO_2 into multicarbon products, such as ethylene, ethanol, and propanol, at substantial rates.[2−4] Despite its capability for CO_2-to-C_{2+} conversion, Cu faces challenges with poor selectivity and stability in CO_2 reduction reaction (CO_2RR).[5−7] The lattice strain, induced by growing a metal overlayer on the substrate, has been used as a common strategy in catalysis to tune the adsorption energies of the reaction intermediate species.[8−13] Such interfacial strain engineering has the potential to tune reaction activity/selectivity while preserving the structural stability of the metal overlayers[14−17] through synergistic effects with the metal substrate. However, synthesizing Cu overlayers on specific metal substrates presents a significant challenge due to the large lattice mismatch (>5%) between Cu and most noble metals[18,19] since the epitaxial growth often requires a < 3% lattice mismatch.[20−22] Although various M@Cu (M = Au, Pt, Pd, etc.) core−shell nanostructures have been successfully synthesized using wet-chemistry methods,[23−27] the Cu overlayers were reported to be thicker than 5 nm to achieve adequate strain relaxation, which behaved like bulk Cu instead of the desirable structure of surface atomic-layer Cu on metal substrates.

Previous reports used the underpotential deposition (UPD) method to alter the catalytic reactivity and selectivity of Cu overlayers for the CO_2RR, which was ascribed to the ligand and strain effects. Chorkendorff et al.[28] and Strasser et al.[29] deposited Cu overlayers on bulk Pt electrodes and quantified the Cu layer thickness by the charge of Cu UPD and bulk

Received: September 10, 2024
Revised: November 27, 2024
Accepted: December 2, 2024
Published: December 16, 2024

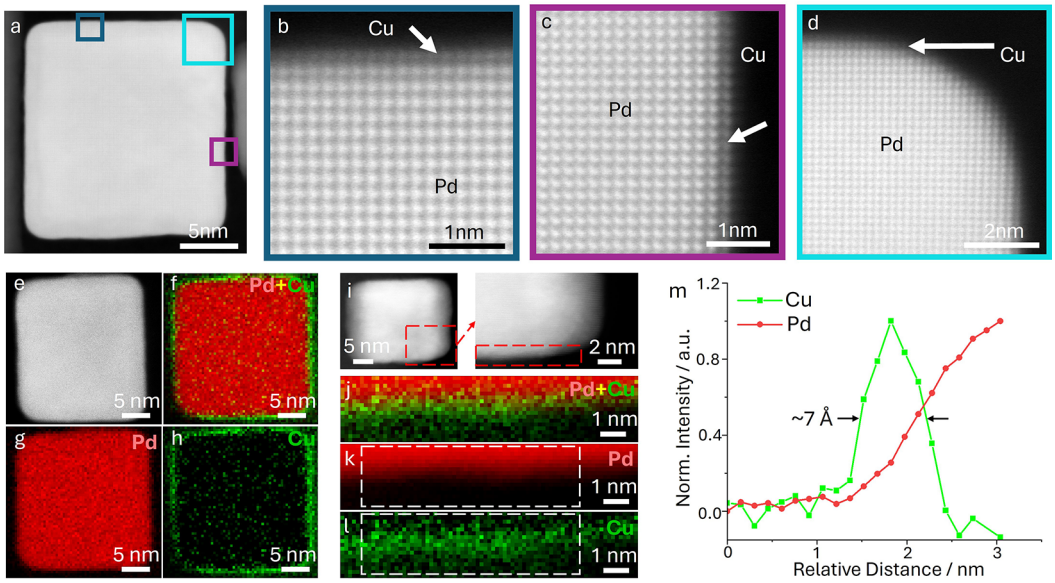

Figure 1. Atomic-scale HAADF-STEM imaging and EELS elemental mapping of Pd@Cu_{atomic} core−shell nanocube. (a) Overall lattice image of a Pd@Cu_{atomic} core−shell nanocube on the zone axis of [100]. (b−d) Atomic-scale STEM images, acquired from the solid box in (a), show a coherent Cu monolayer over the Pd lattice. (e−h) STEM image of a Pd@Cu_{atomic} nanocube and the corresponding EELS elemental maps of Pd (red), Cu (green), and composite map of Pd vs Cu. (i−l) The enlarged EELS elemental mapping, showing atomic-layer Cu on top of the Pd nanocube substrates. (m) EELS line profiles across the Cu/Pd interface show that the Cu shell is ∼7 Å thick.

electrodeposition. Their findings suggest that catalysts with Cu overlayers exhibit higher catalytic activity toward C_{2+} products when compared to bulk Cu catalysts, with a notable effect of the Cu overlayer thickness. Kulesza et al.[30] reported CO_2 electroreduction on multilayered catalysts composed of monolayer Cu covering Pd interlayers deposited on bulk Au (111) electrodes. They found that these overlayer structures exhibited higher catalytic activity toward CO formation than pure Au metal substrates. Those studies involve Cu overlayers on bulk electrodes, which may deviate significantly from practical nanocatalysts. The correlation between the atomic structure of the Cu overlayer and its selectivity/stability for the CO_2RR remains elusive, particularly for high-performance nanocatalysts, due to the lack of atomic-scale characterizations of the Cu/substrate interface.

In this work, Pd@Cu core−shell nanocubes with ∼15 nm and atomic Cu overlayers on ∼20 nm single-crystal Pd nanocubes were synthesized by controlling the deposition rate of Cu^{2+} in aqueous solution. The nanocube morphology was selected in this work to exclusively expose {100} facets on the catalyst surface since early studies on bulk Cu single crystals and Cu nanocubes with {100} facets showed improved CO_2RR selectivity toward C_{2+} products.[5,31,32] We demonstrated the successful epitaxial growth of the atomic-layer Cu on Pd by significantly decreasing the accessible reductant concentration during the nucleation stage. The core−shell structures were evaluated as electrocatalysts for the CO_2RR. Our atomic-scale scanning transmission electron microscopy (STEM) imaging and electron energy-loss spectroscopy (EELS) directly visualize the atomic-layer Cu epitaxially grown on Pd nanocubes, which activate the surface to produce C_{2+} chemicals and remain stable through the course of the CO_2RR. The reaction-driven migration of Cu is effectively suppressed on the Pd substrate due to the strong electronic interaction between Cu and Pd. The thicker Cu shell (∼15 nm) enhances the formation of multicarbon products, relative to Cu nanocube counterparts, but is susceptible to significant structural reconstruction during the reaction.

■ RESULTS AND DISCUSSION

Thick and atomic-layer Cu shells on Pd nanocube cores (Pd@Cu) were synthesized using a seed-mediated wet chemistry method. By introducing ∼20 nm Pd nanocubes into the solution as seeds, precise control over the size and shape of the resulting Pd@Cu core−shell structures could be achieved.[18,33,34] The thickness of Cu shells was controlled by adjusting the reduction rate of the Cu^{2+} precursor through the concentration of the available reductants (ascorbic acid). The Pd@Cu nanocubes with core−shell structures have average sizes of ∼25 nm and ∼50 nm for Pd@Cu_{atomic} and Pd@$Cu_{15\ nm}$, respectively (Figure S1). Atomic-scale high-angle annular dark-field (HAADF) STEM images at the Pd/Cu interface of the Pd@Cu_{atomic} nanocubes revealed the coherent atomic Cu layer on the Pd surface (Figure 1a−d). Pd nanocube core shows a high-quality single-crystal-type structure on the [100] zone axis with *d*-spacings of Pd{200} (1.95 Å). The monolayer Cu, as indicated by arrows in Figure 1b−d, was shown to share nearly the same lattice spacings as Pd substrates, demonstrating the epitaxial relationship between the lattice of Cu and Pd. Given the theoretical 7.7% lattice mismatch between Cu ($d_{\{200\}}$= 1.81 Å) and Pd ($d_{\{200\}}$= 1.95 Å), significant strain within the Cu layer is anticipated as the lattice of Cu adapts to that of Pd (1.95 Å) (Figure S2). Elemental compositions were mapped using atomic-scale STEM-based electron energy-loss spectroscopy (EELS) spectroscopy (Figure 1e−h) and energy dispersive X-ray (EDX) spectroscopy (Figure S3a). STEM-EELS elemental maps of Pd (red, Figure 1g), Cu (green, Figure 1h), and composite map of Pd and Cu (red/green, Figure f) present a uniform atomic Cu overlayer surrounding the Pd core.

EELS mapping acquired from an enlarged region at the Pd core surface validated the presence of an atomic Cu overlayer

https://doi.org/10.1021/acs.chemmater.4c02541
Chem. Mater. 2025, 37, 290−296

(Figure 1i–l), with a thickness of ~7 Å as determined from the EELS line profile (Figure 1m) extracted from the EELS maps (white box in Figure 1k,l). The measured thickness of 7 Å represents the upper limit of the actual thickness of the monolayer Cu, accounting for beam broadening and sample mistilt effects. To the best of our knowledge, this represents the first experimental evidence of an atomically thin Cu layer epitaxially grown on foreign nanocrystal substrates with a lattice mismatch exceeding 5%. The atomically sharp Cu/Pd interface was directly visualized by aberration-corrected HAADF-STEM imaging and EELS elemental mapping.

The ~15 nm Cu layer surrounding the Pd core is clearly visible in EELS and EDX mapping (Figures 2, S3b and S4),

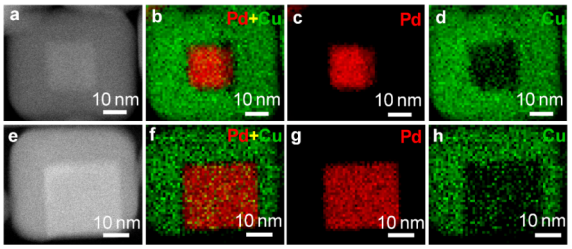

Figure 2. STEM-EELS elemental mapping of Pd@$Cu_{15\ nm}$ core–shell nanocubes. (a–d) STEM image of one Pd@Cu_{atomic} nanocube and the corresponding EELS elemental maps of Pd (red), Cu (green), and composite map of Pd vs Cu, showing an ~15-nm-thick Cu layer evenly deposited on the surface of Pd core. (e–h) STEM image and EELS maps of another nanocube where the Pd core is not centered, indicating the kinetically controlled growth during the initial stages of the growth.

exhibiting the substantial overgrowth of Cu layers along the [100] directions. The shell thickness of the core–shell structure in seed-mediated growth is controlled by the ratio between the rate of deposition and that of surface diffusion of Cu atoms on the Pd surface.[35] For the Pd@$Cu_{15\ nm}$ core–shell nanocubes, Pd seeds were observed to randomly distribute within the nanocubes (as shown by examples in Figures 2e–h, S3b and S4), which is consistent with the previous report when a fast deposition rate of Cu was involved.[24−26] This indicates that the growth of the Cu layer is primarily kinetically controlled during the initial stages of the reaction due to the rapid deposition rate of Cu. As a result, this leads to localized nucleation and growth of Cu on some of the six facets of the Pd nanocube seed. In contrast, when an atomic layer of Cu is synthesized, the concentration of reductants available for the nucleation process is significantly reduced. With a lower quantity and slower deposition rate of Cu, the growth of a thinner and more uniform Cu layer is facilitated by sufficient surface diffusion of Cu on the Pd surface, enabling the formation of a thermodynamically favorable structure.

Following the structural investigation by electron microscopy, the thick Cu layer and the atomic Cu layer on Pd were evaluated as electrocatalysts for the CO_2RR in an H-cell. For comparison, monometallic Pd nanocubes and Cu nanocubes were also tested as control groups (Figure S5). Pd nanocubes mainly produce H_2 and CO, which is consistent with a previous study.[36] In comparison, an atomic Cu layer on the Pd surface is sufficient to initiate the formation of C_2H_4 with a Faradaic efficiency (FE) of 12% (Figure 3a). Increasing the thickness of the Cu layer suppresses the hydrogen evolution reaction (HER) and further enhances the C_{2+} production,

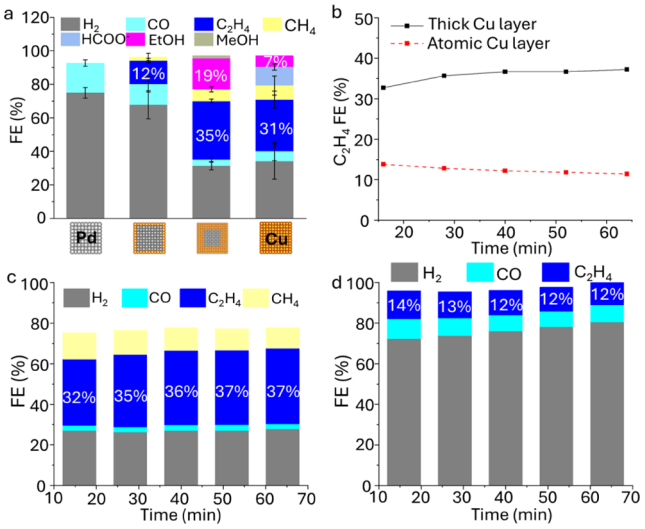

Figure 3. CO_2RR performances of Pd@Cu_{atomic} and Pd@$Cu_{15\ nm}$ core–shell nanocubes. (a) FE for Pd, Pd@Cu_{atomic}, Pd@$Cu_{15\ nm}$, and Cu nanocubes. Measurements were conducted after 1 h chronoamperometry at −1 V vs RHE in 0.1 M $KHCO_3$ solution (pH = 6.8). The C_{2+} products were enhanced by increasing the thickness of the Cu overlayers on Pd, surpassing that measured from monometallic Cu nanocubes. (b) FE of C_2H_4 over ~1 h CO_2RR for the Pd@Cu_{atomic} and Pd@$Cu_{15\ nm}$ core–shell nanocubes. (c) FE stability of gas products over ~1 h CO_2RR for Pd@$Cu_{15\ nm}$, showing an increasing C_2H_4 production over the ~1 h CO_2RR. (d) FE stability of gas products over ~1 h CO_2RR for Pd@Cu_{atomic} with a relatively stable C_2H_4 production.

achieving a total C_{2+} FE of over 50%. Although the ~15 nm Cu layer shows a CO_2-to-C_2H_4 FE of 35%, slightly higher than that of monometallic Cu (31%), there is a significant enhancement in CO_2-to-ethanol FE, with approximately 3-fold higher in the FE toward ethanol when using the Pd@$Cu_{15\ nm}$ (19%) compared to monometallic Cu (7%). It should be noted that the atomic Cu overlayer exhibits lower C_{2+} FE relative to the thick Cu counterpart. This can be attributed to the excessive strain effects of the Cu overlayer, which impact the adsorption of reactive intermediate species due to varying structural and electronic effects.[37−40] It suggests that a Cu overlayer with a moderate thickness might be desired for promoting C_{2+} selectivity. We anticipate an optimal thickness of the Cu layer, providing a moderate electronic effect from the Pd substrate, for optimizing the CO_2RR of the Pd@Cu core–shell structure. This can be reflected in the nonmonotonic trend observed in the plot of C_{2+} FE as a function of Cu content derived from Figure 3a, as a higher C_{2+} selectivity may be expected between the atomic and ~15 nm Cu thickness (Figure S6). The time-dependent FE and partial current density for C_2H_4, measured from an atomic Cu layer, remain relatively stable, as illustrated in Figures 3b and S7. The FE for other gas products was also consistently stable on both thick and atomic Cu layers (Figure 3c,d). A slight increase in C_2H_4 production was observed for the thick Cu layer (Figure S7), indicating potential structural reconstruction of the Cu layer during 1 h CO_2RR.

The compositional distribution of Pd@Cu core–shell nanocubes after the CO_2RR was then examined to assess the structural changes during the CO_2RR. The STEM-EELS mapping of Pd@$Cu_{15\ nm}$ after the CO_2RR reveals significant migration of the Cu shell, leading to severe aggregation of Cu

https://doi.org/10.1021/acs.chemmater.4c02541
Chem. Mater. 2025, 37, 290−296

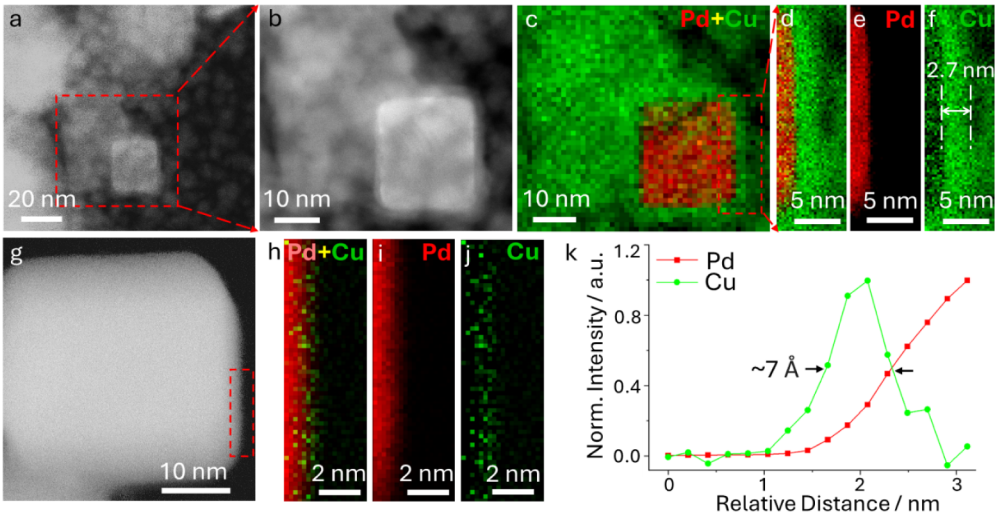

Figure 4. STEM-EELS elemental mapping of Pd@$Cu_{15\ nm}$ and Pd@Cu_{atomic} core−shell nanocubes after 1 h CO_2RR. (a) The overall morphology of the Pd@$Cu_{15\ nm}$ core−shell nanocubes after reaction shows migration of Cu shells, formation of small Cu nanoparticles and aggregation into large Cu clusters. (b) Enlarged HAADF-STEM image of a broken core−shell structure from the magnified view of (a). The Pd core stays stable while the outside Cu layers migrate and reconstruct. (c) EELS maps of Pd (red) vs Cu (green). (d−f) EELS maps of Pd (red), Cu (green) and composite map of Pd vs Cu acquired from the dashed box in (c), revealing a 2.7 nm Cu layer remaining on the Pd surface. (g) HAADF-STEM image of a Pd@Cu_{atomic} core−shell nanocube. (h−j) EELS maps of Pd (red), Cu (green) and composite map of Pd vs Cu acquired from the dashed box in (g), revealing the preservation of the atomic Cu layer of the Pd@Cu_{atomic} structure after the CO_2RR. (k) EELS line profiles corresponding to the EELS maps in (i) and (j) across the surface, indicating a 7 Å thickness Cu layer.

nanoclusters while Pd nanocubes remain largely unchanged (Figures 4a−f and S8−10). This observation aligns with previous studies on Cu nanocatalysts, which demonstrated substantial migration and reconstruction owing to the highly mobile and dynamic nature of Cu atoms during the CO_2RR.[41−43] Interestingly, while the majority of ∼15 nm Cu shell on the Pd surface migrated and aggregated into hundreds of nm Cu clusters, a 2.7 nm thick Cu layer is persistently stable and remains on the Pd surface, as indicated by the high-resolution STEM-EELS mapping (Figure 4f). In other examples of Pd@$Cu_{15\ nm}$ after the CO_2RR, a similar structure of 2−3 nm Cu overlayers were left over and remained on the Pd nanocube surface, which is significantly thinner than the ∼15 nm thick Cu layer observed in the pristine sample (Figures S8 and S9). In addition to the Cu nanoclusters, the high density of small nanoparticles (2−10 nm) at adjacent locations to the Pd nanocubes, was identified as Cu clusters through STEM-EELS analysis (Figure S11). These small nanoparticles are likely a result of the dynamic evolution of the thick Cu shell under reaction conditions, analogous to the observations in the monometallic Cu electrocatalysts during the CO_2RR.[42,44] It is noteworthy that these small Cu nanoparticles were prevented from reaching the Pd surface by the residual 2.7 nm Cu layer, as clearly depicted in Figure 4d. This observation implies a stabilized 2−3 nm Cu layers near the Pd surface remains strongly connected to the Pd surface while the outer section of the Cu shell (around 3 to 15 nm away from the Pd surface) migrates and reconstructs more readily during the CO_2RR. In comparison, the atomic Cu layer of the Pd@Cu_{atom} sample remained stable on the Pd surface after the reaction, as shown in Figure 4g−k. The line profile indicates a Cu overlayer of approximately 7 Å thickness, which is consistent with that observed in the pristine sample (∼7 Å). Similar examples of post-CO_2RR Pd@Cu_{atomic} were provided in Figure S12. Consequently, the stable CO_2RR performance of Pd@Cu_{atomic} (Figure 3b) can be attributed to the stable atomic Cu layer, as confirmed by STEM-EELS analysis. Both the atomic Cu layer and the remaining 2−3 nm Cu layer exhibit the characteristic features of metallic Cu based on the EELS analysis (Figures S13 and S14). The underlying Pd renders the 2−3 nm Cu layer more resistant to air oxidation, likely due to the strong electronic interaction between Cu and Pd.

Based on the structural analysis of the post-CO_2RR, we discovered that 2−3 nm Cu layers appear to be stabilized by the underlying Pd and remain resistant to migration into larger Cu clusters during the CO_2RR. We acknowledge that the structural reasons for the improved C_2H_4 and C_2H_5OH FE of Pd@$Cu_{15\ nm}$ warrant further studies as the active states of catalysts are mixed structures of remaining 2−3 nm Cu overlayers on Pd cubes as well as aggregated Cu nanoclusters. Nevertheless, 2−3 nm Cu layers remaining on the Pd surface present a promising strategy for achieving more stable Cu electrocatalysts for CO_2RR, addressing the stability challenges posed by structural dynamics under reaction conditions, a concern widely recognized within the CO_2RR community.

In conclusion, we have successfully synthesized an atomically thin Cu layer and a ∼15 nm Cu layer on Pd nanocubes by controlling the deposition kinetics of Cu^{2+} in aqueous solution. Atomic-scale HAADF imaging and EELS mapping of Pd@Cu_{atomic} reveal the presence of atomic-layer Cu epitaxially grown on the Pd substrate. We investigated the catalytic performance of CO_2 electroreduction on Pd@Cu_{atomic} and Pd@$Cu_{15\ nm}$ as well as monometallic Cu and Pd nanocube counterparts. The deposition of an atomic Cu layer activates the Pd surface toward the formation of multicarbon products. However, it underperforms compared to the thicker ∼15 nm Cu layers. In comparison, the thicker ∼15 nm Cu overlayers are unstable and have significant reconstruction during the CO_2RR. We reported that a Cu overlayer of intermediate thickness holds significant potential for optimizing both the selectivity and stability of Cu electrocatalysts for CO_2

https://doi.org/10.1021/acs.chemmater.4c02541
Chem. Mater. 2025, 37, 290−296

reduction. Specifically, 2−3 nm Cu layers appear to be stabilized by the underlying Pd and demonstrate resistance to migration during the CO_2RR. The reaction-driven migration of Cu is effectively suppressed on the Pd substrate due to the strong Cu−Pd interaction, which is correlated to the smaller work function value of Cu, relative to Pd.[45] The Cu−Pd interaction is similar to the strong metal−support interaction (SMSI) in oxide-supported metal catalysts.[46] The structural investigation here may also contribute to our understanding of a broad range of bimetallic nanocatalysts for CO_2 reduction.[47−49] We anticipate this study will provide guidelines for designing selective and, more importantly, durable nanocatalysts for electrochemical CO_2 reduction to liquid fuels.

EXPERIMENTAL METHODS

Chemicals. Anhydrous copper(II) chloride ($CuCl_2$), palladium(II) chloride ($PdCl_2$), ascorbic acid (AA), cetyltrimethylammonium bromide (CTAB), hexadecylamine (HDA) were purchased from Sigma-Aldrich. Potassium bicarbonate ($KHCO_3$) (99.99% trace metals basis) was purchased from Aladdin. All the above chemicals were used as received without further purification. All aqueous solutions were prepared using ultrapure deionized water.

Synthesis of Pd Nanocubes. In a typical synthesis, 5 mL of 10 mM H_2PdCl_4 solution was added to 100 mL of 12.5 mM CTAB solution. The mixture was heated at 95 °C under stirring. After 10 min, 800 μL freshly prepared 100 mM ascorbic acid solution was introduced and then stirred for 30 min. The product was collected by centrifugation at 12000 rpm for 10 min, cleaned with deionized water three times to remove the excess CTAB, and redispersed in 40 mL of water for use as seeds.

Synthesis of Pd@Cu Core−Shell Nanocubes. Pd@Cu nanocubes were synthesized via the seed-mediated approach.[18,27] In a typical synthesis of $Pd@Cu_{15\ nm}$, 0.3 g of HDA and 2.5 mL of 0.1 M $CuCl_2$ solution were placed in deionized water in a glass vial and stirred at room temperature overnight. 20 mL aqueous suspension of Pd seeds was added to the Cu precursor solution. The mixture was heated to 90 °C in an oil bath, following the one-shot injection of 1 mL of 1 M AA solution. The reaction proceeded at 90 °C for 1 h in an oil bath and naturally cooled to room temperature. The products were separated from the solution by centrifuging at 8000 rpm for 10 min and washed three times with deionized water and ethanol to remove the excess HDA. For the synthesis of $Pd@Cu_{atomic}$, the amount of Cu^{2+} was reduced to 0.05 mmol, and the injection rate of 1 mL of 0.2 M AA solution was controlled to be 1.5 μL/s to slow down the deposition rate of Cu^{2+}. The products were finally redispersed in deionized water for storage.

Structural Characterizations. HAADF-STEM imaging and EELS were conducted using an aberration-corrected Thermo Fisher Scientific Titan Themis (S)TEM, operating at 300 keV. HAADF-STEM images in Figure 1a−d were acquired at 300 kV, and the dwell time is 10 μs at each scan position. EELS spectral images were obtained with a beam convergence semiangle of 30 mrad, utilizing a Gatan spectrometer. Elemental maps for Cu and Pd were generated by extracting data from the Cu L and Pd M edges in the EELS spectrum images. The spectra were processed using the principal component analysis (PCA, with 3 components) and the linear combination of power law (LCPL) for background subtraction in ImageJ software. EDX measurements were performed on a JEOL ARM 200CF equipped with an Oxford Instruments X-ray energy-dispersive spectrometer. For the postreaction TEM characterization, a lacey carbon TEM grid was pressed onto the glassy carbon electrode with a drop of ethanol atop for several seconds to collect the reacted nanoparticles after electrolysis.

CO_2RR Performance Test. All performance tests were conducted using an H-cell at room temperature, with a glassy carbon electrode as the working electrode, a platinum mesh as the counter electrode, and a saturated Ag/AgCl electrode as the reference electrode. Approximately 50 μg of catalyst, suspended in ethanol, was drop-cast onto a 1 cm^2 area of the glassy carbon electrode. The electrolyte was CO_2-saturated 0.1 M $KHCO_3$, with CO_2 continuously purged at 20 sccm throughout the tests. Details of GC and NMR analysis can be found in experimental sections.

ASSOCIATED CONTENT

Supporting Information

The Supporting Information is available free of charge at https://pubs.acs.org/doi/10.1021/acs.chemmater.4c02541.

GC and NMR analysis. STEM-EELS analysis of pristine and post-CO_2RR Pd@Cu core−shell nanoparticles and CO_2RR performance (Figures S1−S15) (PDF)

AUTHOR INFORMATION

Corresponding Authors

Yimo Han − *Department of Materials Science and Nano Engineering, Rice University, Houston, Texas 77005, United States;* orcid.org/0000-0003-0563-4611; Email: yh76@rice.edu

Yao Yang − *Department of Chemistry and Chemical Biology, Cornell University, Ithaca, New York 14853, United States;* orcid.org/0000-0003-0321-3792; Email: yaoyang@cornell.edu

Authors

Shikai Liu − *Department of Chemistry and Chemical Biology, Cornell University, Ithaca, New York 14853, United States*

Chuqiao Shi − *Department of Materials Science and Nano Engineering, Rice University, Houston, Texas 77005, United States*

Chaokai Xu − *Department of Material Science and Engineering, College of Design and Engineering, National University of Singapore, Singapore 117575, Singapore;* orcid.org/0000-0001-8366-888X

Haichuan Zhang − *Department of Chemistry and Chemical Biology, Cornell University, Ithaca, New York 14853, United States*

Wenqi Li − *Department of Chemistry and Chemical Biology, Cornell University, Ithaca, New York 14853, United States*

Valentín Briega-Martos − *Department of Chemistry and Chemical Biology, Cornell University, Ithaca, New York 14853, United States;* orcid.org/0000-0001-8407-2260

Qian He − *Department of Material Science and Engineering, College of Design and Engineering, National University of Singapore, Singapore 117575, Singapore*

Complete contact information is available at: https://pubs.acs.org/10.1021/acs.chemmater.4c02541

Author Contributions

#S.L. and C.S. contributed equally.

Notes

The authors declare no competing financial interest.

ACKNOWLEDGMENTS

This work was supported by the Center for Alkaline-Based Energy Solutions (CABES), an Energy Frontier Research Center (EFRC) program supported by the U.S. Department of Energy, under grant DE-SC0019445. This work was supported by the Cornell Atkinson Center for Sustainability and the 2030 Project: A Cornell Climate Initiative. This work made use of TEM facilities at the CCMR, which are supported through the National Science Foundation Materials Research Science and

Engineering Center (NSF MRSEC) program (DMR-1719875). C.S. and Y.H. acknowledge NSF (CMMI−2239545), Welch Foundation (C-2065), and American Chemical Society Petroleum Research Fund (67236-DNI10). We thank Y. Hu and Prof. Andrew Wong from National University of Singapore with the help of CO_2RR performance tests. We dedicate this work to Prof. Francis J. DiSalvo (Frank) at Cornell Chemistry and are honored to carry on his legacy on solid-state chemistry of energy materials.

REFERENCES

(1) Kondratenko, E. V.; Mul, G.; Baltrusaitis, J.; Larrazábal, G. O.; Pérez-Ramírez, J. Status and Perspectives of CO_2 Conversion into Fuels and Chemicals by Catalytic, Photocatalytic and Electrocatalytic Processes. *Energy Environ. Sci.* **2013**, *6* (11), 3112.

(2) Birdja, Y. Y.; Pérez-Gallent, E.; Figueiredo, M. C.; Göttle, A. J.; Calle-Vallejo, F.; Koper, M. T. M. Advances and Challenges in Understanding the Electrocatalytic Conversion of Carbon Dioxide to Fuels. *Nat. Energy* **2019**, *4* (9), 732−745.

(3) Ross, M. B.; De Luna, P.; Li, Y.; Dinh, C.-T.; Kim, D.; Yang, P.; Sargent, E. H. Designing Materials for Electrochemical Carbon Dioxide Recycling. *Nat. Catal.* **2019**, *2* (8), 648−658.

(4) Gao, D.; Arán-Ais, R. M.; Jeon, H. S.; Roldan Cuenya, B. Rational Catalyst and Electrolyte Design for CO_2 Electroreduction towards Multicarbon Products. *Nat. Catal.* **2019**, *2* (3), 198−210.

(5) Grosse, P.; Yoon, A.; Rettenmaier, C.; Herzog, A.; Chee, S. W.; Roldan Cuenya, B. Dynamic Transformation of Cubic Copper Catalysts during CO_2 Electroreduction and its Impact on Catalytic Selectivity. *Nat. Commun.* **2021**, *12* (1), 6736.

(6) Popovic, S.; Smiljanic, M.; Jovanovic, P.; Vavra, J.; Buonsanti, R.; Hodnik, N. Stability and Degradation Mechanisms of Copper-Based Catalysts for Electrochemical $CO_{(2)}$ Reduction. *Angew. Chem., Int. Ed.* **2020**, *59* (35), 14736−14746.

(7) Kim, D.; Kley, C. S.; Li, Y.; Yang, P. Copper Nanoparticle Ensembles for Selective Electroreduction of $CO_{(2)}$ to $C_{(2)}$-$C_{(3)}$ Products. *Proc. Natl. Acad. Sci. U. S. A.* **2017**, *114* (40), 10560−10565.

(8) Kitchin, J. R.; Norskov, J. K.; Barteau, M. A.; Chen, J. G. Role of Strain and Ligand Effects in the Modification of the Electronic and Chemical Properties of Bimetallic Surfaces. *Phys. Rev. Lett.* **2004**, *93* (15), 156801.

(9) Strasser, P.; Koh, S.; Anniyev, T.; Greeley, J.; More, K.; Yu, C.; Liu, Z.; Kaya, S.; Nordlund, D.; Ogasawara, H.; et al. Lattice-Strain Control of the Activity in Dealloyed Core-Shell Fuel Cell Catalysts. *Nat. Chem.* **2010**, *2* (6), 454−460.

(10) Zhang, J.; Vukmirovic, M. B.; Xu, Y.; Mavrikakis, M.; Adzic, R. R. Controlling the Catalytic Activity of Platinum-Monolayer Electrocatalysts for Oxygen Reduction with Different Substrates. *Angew. Chem., Int. Ed.* **2005**, *44* (14), 2132−2135.

(11) Wang, J.; Inada, H.; Wu, L.; Zhu, Y.; Choi, Y.; Liu, P.; Zhou, W.; Adzic, R. R. Oxygen Reduction on Well-Defined Core-Shell Nanocatalysts: Particle Size, Facet, and Pt Shell Thickness Effects. *J. Am. Chem. Soc.* **2009**, *131*, 17298−17302.

(12) Jiang, G.; Zhu, H.; Zhang, X.; Shen, B.; Wu, L.; Zhang, S.; Lu, G.; Wu, Z.; Sun, S. Core/Shell Face-Centered Tetragonal FePd/Pd Nanoparticles as an Efficient Non-Pt Catalyst for the Oxygen Reduction Reaction. *ACS Nano* **2015**, *9*, 11014−11022.

(13) Xie, M.; Lyu, Z.; Chen, R.; Shen, M.; Cao, Z.; Xia, Y. Pt-Co@Pt Octahedral Nanocrystals: Enhancing Their Activity and Durability toward Oxygen Reduction with an Intermetallic Core and an Ultrathin Shell. *J. Am. Chem. Soc.* **2021**, *143* (22), 8509−8518.

(14) Foucher, A. C.; Rosen, D. J.; Decker, L. K.; Macfarlane, R. J.; Murray, C. B.; Stach, E. A.; Ross, F. M. Structure and Stability of Core−Shell Cu−Pt Nanoparticles for Catalytic Applications. *Chem. Mater.* **2023**, *35* (20), 8758−8764.

(15) Zhang, Y.; Lyu, Z.; Chen, Z.; Zhu, S.; Shi, Y.; Chen, R.; Xie, M.; Yao, Y.; Chi, M.; Shao, M.; et al. Maximizing the Catalytic Performance of Pd@$Au_{(x)}$ $Pd_{(1-x)}$ Nanocubes in $H_{(2)}$ $O_{(2)}$ Production by Reducing Shell Thickness to Increase Compositional Stability. *Angew. Chem., Int. Ed.* **2021**, *60* (36), 19643−19647.

(16) Chen, D.; Li, C.; Liu, H.; Ye, F.; Yang, J. Core-shell Au@Pd nanoparticles with enhanced catalytic activity for oxygen reduction reaction via core-shell Au@Ag/Pd constructions. *Sci. Rep.* **2015**, *5*, 11949.

(17) Niu, Z.; Cui, F.; Yu, Y.; Becknell, N.; Sun, Y.; Khanarian, G.; Kim, D.; Dou, L.; Dehestani, A.; Schierle-Arndt, K.; et al. Ultrathin Epitaxial Cu@Au Core-Shell Nanowires for Stable Transparent Conductors. *J. Am. Chem. Soc.* **2017**, *139* (21), 7348−7354.

(18) Jin, M.; Zhang, H.; Wang, J.; Zhong, X.; Lu, N.; Li, Z.; Xie, Z.; Kim, M. J.; Xia, Y. Copper Can Still Be Epitaxially Deposited on Palladium Nanocrystals To Generate Core@Shell Nanocubes Despite Their Large Lattice Mismatch. *ACS Nano* **2012**, *6*, 2566−2573.

(19) Fan, F.; Liu, D.; Wu, Y.; Duan, S.; Xie, Z.; Jiang, Z.; Tian, Z. Epitaxial Growth of Heterogeneous Metal Nanocrystals: From Gold Nano-octahedra to Palladium and Silver Nanocubes. *J. Am. Chem. Soc.* **2008**, *130*, 6949−6951.

(20) Eom, C. J.; Kuo, D. Y.; Adamo, C.; Moon, E. J.; May, S. J.; Crumlin, E. J.; Schlom, D. G.; Suntivich, J. Tailoring Manganese Oxide with Atomic Precision to Increase Surface Site Availability for Oxygen Reduction Catalysis. *Nat. Commun.* **2018**, *9* (1), 4034.

(21) Yang, Y.; Zeng, R.; Paik, H.; Kuo, D.-Y.; Schlom, D. G.; DiSalvo, F. J.; Muller, D. A.; Suntivich, J.; Abruña, H. D. Epitaxial Thin-Film Spinel Oxides as Oxygen Reduction Electrocatalysts in Alkaline Media. *Chem. Mater.* **2021**, *33* (11), 4006−4013.

(22) Shi, C.; Cheng, Z.; Leonardi, A.; Yang, Y.; Engel, M.; Jones, M. R.; Han, Y. Preserving Surface Strain in Nanocatalysts via Morphology Control. *Sci. Adv.* **2024**, *10* (39), adp378.

(23) Tsuji, M.; Yamaguchi, D.; Matsunaga, M.; Alam, M. J. Epitaxial Growth of Au@Cu Core−Shell Nanocrystals Prepared Using the PVP-Assisted Polyol Reduction Method. *Cryst. Growth Des.* **2010**, *10* (12), 5129−5135.

(24) Wang, Z.; Chen, Z.; Zhang, H.; Zhang, Z.; Wu, H.; Jin, M.; Wu, C.; Yang, D.; Yin, Y. Lattice-Mismatch-Induced Twinning for Seeded Growth of Anisotropic Nanostructures. *ACS Nano* **2015**, *9*, 3307−3313.

(25) Hsia, C.-F.; Madasu, M.; Huang, M. H. Aqueous Phase Synthesis of Au−Cu Core−Shell Nanocubes and Octahedra with Tunable Sizes and Noncentrally Located Cores. *Chem. Mater.* **2016**, *28* (9), 3073−3079.

(26) Lyu, Z.; Xie, M.; Aldama, E.; Zhao, M.; Qiu, J.; Zhou, S.; Xia, Y. Au@Cu Core−Shell Nanocubes with Controllable Sizes in the Range of 20−30 nm for Applications in Catalysis and Plasmonics. *ACS Appl. Nano Mater.* **2019**, *2* (3), 1533−1540.

(27) Zhang, G.; Feng, J.; Wang, S.; Xu, B.; Ding, W.; Wang, W.; Fu, Z. Stable Pd@Cu Core−Shell Nanocubes with Finely Tuned Sizes for the Reduction of Nitroaromatics. *ACS Appl. Nano Mater.* **2019**, *2* (7), 4584−4593.

(28) Varela, A. S.; Schlaup, C.; Jovanov, Z. P.; Malacrida, P.; Horch, S.; Stephens, I. E. L.; Chorkendorff, I. CO_2 Electroreduction on Well-Defined Bimetallic Surfaces: Cu Overlayers on Pt(111) and Pt(211). *J. Phys. Chem. C* **2013**, *117* (40), 20500−20508.

(29) Reske, R.; Duca, M.; Oezaslan, M.; Schouten, K. J. P.; Koper, M. T. M.; Strasser, P. Controlling Catalytic Selectivities during CO_2 Electroreduction on Thin Cu Metal Overlayers. *J. Phys. Chem. C* **2013**, *4* (15), 2410−2413.

(30) Januszewska, A.; Jurczakowski, R.; Kulesza, P. J. $CO_{(2)}$ Electroreduction at Bare and Cu-Decorated Pd Pseudomorphic Layers: Catalyst Tuning by Controlled and Indirect Supporting onto Au(111). *Langmuir* **2014**, *30* (47), 14314−14321.

(31) Huang, J.; Hormann, N.; Oveisi, E.; Loiudice, A.; De Gregorio, G. L.; Andreussi, O.; Marzari, N.; Buonsanti, R. Potential-induced nanoclustering of metallic catalysts during electrochemical CO_2 reduction. *Nat. Commun.* **2018**, *9* (1), 3117.

(32) Hori, Y.; Takahashi, I.; Koga, O.; Hoshi, N. Selective Formation of C_2 Compounds from Electrochemical Reduction of CO_2 at a Series of Copper Single Crystal Electrodes. *J. Phys. Chem. B* **2002**, *106*, 15−17.

https://doi.org/10.1021/acs.chemmater.4c02541
Chem. Mater. 2025, 37, 290−296

(33) Jin, M.; Zhang, H.; Xie, Z.; Xia, Y. Palladium Concave Nanocubes with High-index Facets and their Enhanced Catalytic Properties. *Angew. Chem., Int. Ed.* **2011**, *50* (34), 7850−7854.
(34) Murphy, C. J.; Sau, T. K.; Gole, A. M.; Orendorff, C. J.; Gao, J.; Gou, L.; Hunyadi, S. E.; Li, T. Anisotropic Metal Nanoparticles: Synthesis, Assembly, and Optical Applications. *J. Phys. Chem. B* **2005**, *109*, 13857−13870.
(35) Xia, Y.; Xia, X.; Peng, H. C. Shape-Controlled Synthesis of Colloidal Metal Nanocrystals: Thermodynamic versus Kinetic Products. *J. Am. Chem. Soc.* **2015**, *137* (25), 7947−7966.
(36) Gao, D.; Zhou, H.; Wang, J.; Miao, S.; Yang, F.; Wang, G.; Wang, J.; Bao, X. Size-dependent Electrocatalytic Reduction of CO_2 over Pd Nanoparticles. *J. Am. Chem. Soc.* **2015**, *137* (13), 4288−4291.
(37) Wang, J. X.; Inada, H.; Wu, L.; Zhu, Y.; Choi, Y.; Liu, P.; Zhou, W. P.; Adzic, R. R. Oxygen Reduction on Well-Defined Core-Shell Nanocatalysts: Particle Size, Facet, and Pt Shell Thickness Effects. *J. Am. Chem. Soc.* **2009**, *131*, 17298−17302.
(38) Mazumder, V.; Chi, M.; More, K. L.; Sun, S. Core/Shell Pd/FePt Nanoparticles as an Active and Durable Catalyst for the Oxygen Reduction Reaction. *J. Am. Chem. Soc.* **2010**, *132*, 7848−7849.
(39) Choi, R.; Choi, S. I.; Choi, C. H.; Nam, K. M.; Woo, S. I.; Park, J. T.; Han, S. W. Designed Synthesis of Well-defined Pd@Pt Core-shell Nanoparticles with Controlled Shell Thickness as Efficient Oxygen Reduction Electrocatalysts. *Chemistry* **2013**, *19* (25), 8190−8198.
(40) Bando, Y.; Takahashi, Y.; Ueta, E.; Todoroki, N.; Wadayama, T. Electrochemical Properties of Pt Epitaxial Layers Formed on Pd(111) in Ultra-High Vacuum. *J. Electrochem. Soc.* **2015**, *162* (4), F463−F467.
(41) Yang, Y.; Louisia, S.; Yu, S.; Jin, J.; Roh, I.; Chen, C.; Fonseca Guzman, M. V.; Feijoo, J.; Chen, P. C.; Wang, H.; et al. Operando Studies Reveal Active Cu Nanograins for $CO(_2)$ Electroreduction. *Nature* **2023**, *614* (7947), 262−269.
(42) Yang, Y.; Shi, C.; Feijoo, J.; Jin, J.; Chen, C.; Han, Y.; Yang, P. Dynamic Evolution of Copper Nanowires during $CO(_2)$ Reduction Probed by Operando Electrochemical 4D-STEM and X-ray Spectroscopy. *J. Am. Chem. Soc.* **2024**, *146* (33), 23398−23405.
(43) Amirbeigiarab, R.; Tian, J.; Herzog, A.; Qiu, C.; Bergmann, A.; Roldan Cuenya, B.; Magnussen, O. M. Atomic-scale Surface Restructuring of Copper Electrodes under CO_2 Electroreduction Conditions. *Nat. Catal.* **2023**, *6* (9), 837−846.
(44) Liu, S.; Li, Y.; Wang, D.; Xi, S.; Xu, H.; Wang, Y.; Li, X.; Zang, W.; Liu, W.; Su, M.; et al. Alkali Cation-induced Cathodic Corrosion in Cu electrocatalysts. *Nat. Commun.* **2024**, *15* (1), 5080.
(45) Rumble, J. *CRC Handbook of Chemistry and Physics version 2008*; CRC Press; pp. 2−124.
(46) Liu, J. Advanced Electron Microscopy of Metal−Support Interactions in Supported Metal Catalysts. *ChemCatchem* **2011**, *3*, 934.
(47) Chen, P. C.; Chen, C.; Yang, Y.; Maulana, A. L.; Jin, J.; Feijoo, J.; Yang, P. Chemical and Structural Evolution of AgCu Catalysts in Electrochemical CO_2 Reduction. *J. Am. Chem. Soc.* **2023**, *145* (18), 10116−10125.
(48) Chen, C.; Yu, S.; Yang, Y.; Louisia, S.; Roh, I.; Jin, J.; Chen, S.; Chen, P.-C.; Shan, Y.; Yang, P. Exploration of the Bio-analogous Asymmetric C−C Coupling Mechanism in Tandem CO_2 Electroreduction. *Nat. Catal.* **2022**, *5* (10), 878−887.
(49) Ma, S.; Sadakiyo, M.; Heima, M.; Luo, R.; Haasch, R. T.; Gold, J. I.; Yamauchi, M.; Kenis, P. J. Electroreduction of Carbon Dioxide to Hydrocarbons Using Bimetallic Cu-Pd Catalysts with Different Mixing Patterns. *J. Am. Chem. Soc.* **2017**, *139* (1), 47−50.

https://doi.org/10.1021/acs.chemmater.4c02541
Chem. Mater. 2025, 37, 290−296